Macromolecules

ARTICLE

pubs.acs.org/Macromolecules

The Possible Scalability of Mesophase Separation on Macrophase Separation and Crystallization of iPP/OBC Blends

Jing Jin, Chuanzhuang Zhao, Jiang Du,* and Charles C. Han*

State Key Laboratory of Polymer Physics and Chemistry, Joint Laboratory of Polymer Science and Materials, Institute of Chemistry, Chinese Academy of Sciences, Beijing 100190, China

ABSTRACT: This work focuses on the effect of the unique molecular structure of OBC (olefin block copolymer) constituted by soft blocks and hard blocks on the compatibility of OBC/iPP (isotactic polypropylene) blends. Two OBCs with high and low octene content were selected to blend with iPP. The thermal behavior, morphology, and kinetics of crystallization of the binary blends were studied systematically. The variation in octene content of the OBCs caused a dramatic difference in their own mesophase separation as well as their compatibility with iPP in blends. As the octene content increased, mesophase separation of OBC became more and more dominant, with the strong repulsive interaction between the hard and soft blocks of OBC and the coupled fact that the majority of the soft blocks are more compatible with iPP, resulting in its better compatibility with iPP. This was proved by smaller dispersed domain size, better interfacial adhesion, and faster crystallization kinetics. On the other hand, we also found that annealing time was important in controlling the superstructure in blends. There is a possible scalability of the mesophase separation of OBC on the compatibility and superstructure of the OBC/iPP binary blends. According to our results, it is reasonable to obtain a systematic profile to adjust the compatibility as well as the superstructure to satisfy different mechanical requirement by regulating octene content in the OBC and the annealing condition of the blends.

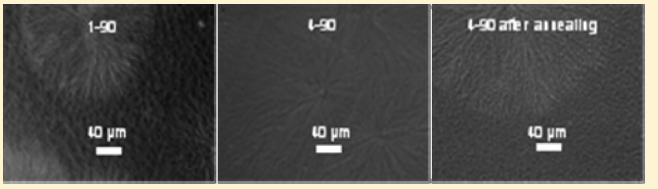

INTRODUCTION

The need to optimize mechanical properties and reduce process cost has motivated the development of polyolefin blends for several decades, as blending is indeed a convenient and efficient route for the development of new materials benefiting from a synergetic effect from the individual components.[1,2] Blends that incorporate one or more crystallizable components have received continuing attention as they offer an effective route to novel property profiles.[3−5] It is well-known that iPP (isotactic polypropylene) has poor impact resistance, especially at low temperature and/or high impact rates, which limits its applications in engineering areas. Consequently, many efforts have explored blending varieties of elastomers with iPP to improve its impact toughness.[6−13] As the properties of crystallizable blends not only are determined by the miscibility between or among the components but also depend to a large extent on their crystalline superstructure and morphology, the compatibility between components is crucial in tuning the properties of the blends. In most cases, block copolymer was added into the blend system to improve the interfacial adhesion between the secondary component and iPP serving as some kind of compatibilizer. Although a large amount of experimental data on iPP blends with two or ternary composites has been published,[8−10] experimental data on miscibility of a block copolymer with iPP are very scarce, especially with a novel statistical multiblock copolymer.[11,14]

Recently, Dow Chemical has made a new olefin block copolymer (OBC) via a process called chain shuttling polymerization.[14] These blocky copolymers consist of crystallizable ethylene−octene blocks with low octene content and high melting temperature (hard blocks), alternating with amorphous ethylene−octene blocks with high octene content and low glass transition temperature (soft blocks). Since OBC is a single-component system with polydispersity, there is only one phase in the macroscopic limit (or the thermodynamic limit) at constant temperature and pressure, this is determined by the phase rule and is true for any block copolymers. Its phase separation can only happen in the sub-macroscale, which is the mesoscale and/or microscale at a condition below the MST (mesophase separation transition) temperature. Normally, block copolymers have a well-defined microphase separation, but due to the nature of the multiblock copolymers with distribution in number of blocks, molecular weight, comonomers composition, and sequence length,[15] OBCs have less defined microphase separation as typical di- or triblock copolymers do; it is more likely that some similar blocks aggregate into mesoscaled phase separation. In terms of structure, OBC is like a composition fluctuation-induced mesophase separation without a clearly defined interphase, nor an ordered structure as there is also a distribution of the domain size. (Here, we emphasize the difference of the microphase/mesophase separation between the traditional block copolymer and the polydispersed OBCs.) The details about the one component OBC's phase behavior have been discussed in our previous work.[16] It was found that as the octene content increased, mesophase separation

Received: January 28, 2011
Revised: April 18, 2011
Published: May 06, 2011

Table 1. Characteristics of OBCs[a]

sample	M_w (g/mol)	M_n (g/mol)	net octene content (mol %)	soft block octene content (mol %)	hard block octene content (mol %)	wt % of soft segment
OBC1	179 000	76 000	17.9	22.6	1.13	84
OBC4	249 000	74 000	25.4	35.7	2.10	82

[a] Data were provided by The Dow Chemical Company.

between hard blocks and soft blocks becomes more and more dominant and the crystal morphology degrades gradually from spherulites to dispersed relaxed lamellar structures. When the mesophase separation is the dominant process, the formed spherical mesophase-separated domains maintain a dispersed state even after crystallization. Crystal lamellae could only grow through the interstitial space of these mesophase-separated domains.

Since an OBC is a multiblock copolymer with a statistical distribution in the molecular structure,[15] the competitive interactions between incompatible blocks in OBC and between these blocks and iPP homopolymer molecules can give rise to a special phase behavior of such blends and affect their phase separation, morphology, and properties. Considering all the above, it is essential to study the phase behavior of the iPP/OBC blends systematically.

Blends of an AB copolymer with a homopolymer A (or B) and blends of an AB copolymer with a homopolymer C which is selectively miscible with the A (or B) homopolymers have been studied extensively.[1,17,18] Furthermore, blends comprised of a diblock copolymer with a homopolymer having similar molecular structure or some special interaction with at least one of the blocks have been well studied,[19−24] and the research on the well-designed block copolymer/homopolymer system has caused attention recently.[22−24] However, most of these studies focused on the effect of the homopolymer on the characteristic dimensions and morphology of the self-assembled structures of the block copolymers. In our present study, no strong specific interactions (like hydrogen bonding or ionic effect) are occurring in OBC/iPP, which exhibits macrophase separation in all blends considered. From our efforts to determine the differences in compatibility between iPP and OBC from morphological and kinetic standpoints as the octene content in OBC varied, we could conclude that OBCs' molecular and mesophase separation structures have a dramatic influence on the macrophase separation and crystallization of such blends.

EXPERIMENTAL SECTION

OBCs synthesized by the chain-shuttling technology were kindly supplied as pellets by The Dow Chemical Company. The molecular parameters of the OBCs used are presented in Table 1. iPP (trademarked as S1003) with $M_w = 3.4 \times 10^5$ g/mol and $M_w/M_n = 3.8$ is a commercial product purchased from Beijing Yanshan Petrochemical Co., Ltd.

To prepare blends, iPP and OBC were dissolved in xylene with a polymer mass composition of ca. 1% at 130 °C for 24 h and then coprecipitated from this hot xylene solution into a large excess of methanol at room temperature. After filtration, the blends were dried in air for 24 h and further dried in a vacuum oven at room temperature for 3 days. For comparison, plain iPP component was also prepared by the same procedure. OBC weight fractions of 0.10, 0.50, and 0.90 were used in these blends, which are named as 1-10, 1-50, 1-90 in the OBC1/iPP blends (blend1) and 4-10, 4-50, 4-90 in the OBC4/iPP blends (blend4).

Thermograms were obtained on a Mettler Toledo-822e differential scanning calorimeter (DSC). Specimens weighing 5−10 mg were picked from samples for thermal analysis. The thermal behavior is studied between 30 and 200 °C with a heating/cooling rate of 10 °C/min. All the measurements were conducted under nitrogen with a flow rate of 20 mL/min.

The optical microscopy (OM) observations were carried out using an Olympus (BX51) optical microscope and Olympus (C-5050ZOOM) camera. A Linkam (350) hot stage was used to control the experimental temperature. Films (~30 μm) of the blends were prepared by hot pressing at 200 ± 2 °C between two glass slides. For a typical OM experiment, the blend was first annealed at 200 °C for 5 min to erase thermal history, then quenched to 140 °C at 30 °C/min and held at that temperature for 6 h, and finally cooled to room temperature at 10 °C/min. The radius of the dendrites was measured by ImageJ software, and the linear growth rate of dendrite was derived from the slope of the dendrite radius over time plot. The consistency of the growth rate has been checked by taking five measurements for each sample; due to the nucleation and growth nature, the radius data cannot be averaged, and only the medium sized dendrite data are plotted here. For the experiment of annealing at 200 °C for 12 h, the sandwiched specimens were surrounded with silicon oil to avoid the thermal degradation of the polymer.

Specimens for atomic force microscopy (AFM) imaging were prepared from the samples tested by OM. After cooling to room temperature, the cover glass slide was removed in liquid nitrogen; the free surface was imaged in air with a commercial scanning probe microscope (Nanoscope III) from Digital Instruments operated in tapping mode. Images were collected at ambient conditions.

The samples after OM or AFM tests were etched in *n*-heptane at ambient temperature for 1 week to wash out the more soluble component of OBC, and then the film was coated with platinum prior to examination by a scanning electron microscope (SEM). A JEOL (JSM 6700F) SEM was used with an operating voltage of 5 kV for this study.

RESULTS AND DISCUSSION

In the present work, with the aim to study the compatibility between OBCs and iPP by comparing phase behavior between the OBC1/iPP and OBC4/iPP blends, we focus on the blends with the asymmetrical volume fractions which contain 10 and 90 wt % OBCs, the typical thermal traces obtained from the DSC measurement are shown in Figure 1. The left traces show the crystallization during the cooling, while the subsequent melting curves of these blends were compiled on the right. The crystallization and melting curves of pure iPP and OBCs are also provided for comparison.

Seen from Figure 1a, the pure OBCs show crystallization peaks at 87 °C (OBC1) and 74 °C (OBC4), while all blends exhibit a single crystallization peak. We have previously reported the crystallization behavior of pure OBCs in detail.[16] OBCs have little effect on the crystallization behavior of iPP in the 10/90 OBC/iPP blends, as evidenced by the similar peak to plain iPP at 114 °C. On the other hand, the crystallization of iPP must be considerably retarded by the existence of 90 wt % OBC component in blends, as evidenced by the depression in temperature and area of the crystallization peaks. Meanwhile, it can be assumed that the preformed crystals of iPP will serve as nuclei

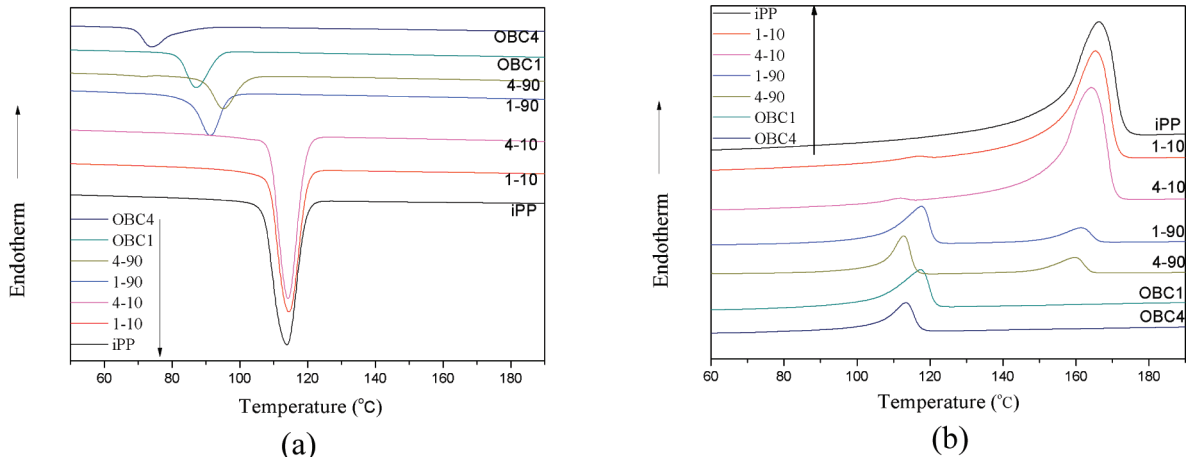

Figure 1. Thermal behavior of the samples: (a) the crystallization process; (b) the melting process. The scan rate was 10 °C/min. The samples were annealed at 200 °C for 5 min, then cooled to 30 °C at 10 °C/min to obtain the crystallization curves (a), and reheated to 200 °C at the same rate to obtain the melting curves (b).

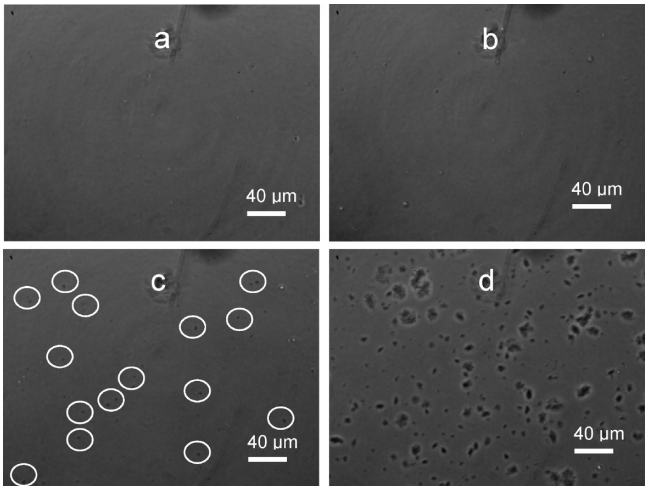

Figure 2. Phase contrast optical micrographs of nonisothermal crystalline morphology: (a) OBC1, (b) OBC4, (c) 1-90, and (d) 4-90. These micrographs were taken at 110 °C during cooling from 200 to 30 °C at 10 °C/min. The circles in (c) are drawn to guide the eyes for the iPP nuclei.

for OBC to assist it to crystallize, resulting in an overlapped crystallization peak here.

In contrast to the crystallization behavior, there are two distinguishable melting peaks for all of the blends in the subsequent heating process as shown in Figure 1b. The peak at 166 °C corresponds to the melting of iPP which is characteristic of the melting of the α-form of iPP. The melting peaks at 118 and 114 °C are attributed to the melting of hard blocks in OBC1 and OBC4 individually, as the temperatures are typical for the melting of low density linear polyethylene.

It is interesting to note that 4-90 has a higher crystallization temperature than 1-90 even though OBC4 has a lower crystallization temperature than OBC1. In this case, one might anticipate a particular effect between OBC4 and iPP which enhances the crystallization in 4-90 compared with 1-90. In order to explain this seemingly confusing nonisothermal crystallization behavior between 1-90 and 4-90, the corresponding crystallization morphologies of the relative samples after identical heat treatment as in the DSC measurements are observed by OM, as shown in Figure 2. From the DSC data for the pure iPP and pure OBCs, it is clear that any component has crystallized upon cooling to 30 °C. However, at 110 °C, the DSC data indicate that the pure OBCs have not yet crystallized and this is supported by the OM micrographs of Figure 2a,b. In contrast, the OM micrographs for 1-90 and 4-90 (Figures 2c and 2d, respectively) show crystallization within the blends at 110 °C, despite the lack of any signature of crystallization in the DSC data. On the basis of the higher melting temperature of iPP crystals observed on reheating these blends, we attribute the crystallization at 110 °C to that of iPP. In addition, the crystallization is markedly different between the two blends. In Figure 2c, several iPP crystals appear as tiny dark spots in the phase contrast graphs (marked in the white circles), while in Figure 2d, significantly more and larger dendrites are formed. This result indicates an enhanced ability to nucleate in 4-90, which is consistent with the higher crystallization temperature of 4-90 than 1-90. The particular mechanism[25,26] of nucleation in OBC/iPP blends will be discussed in detail elsewhere.

The optical micrographs of the blends and the pure OBCs cooled to room temperature following annealing at 140 °C for 6 h are compiled in Figure 3. It is clear to see the remarkable difference between the two OBCs by comparing Figures 3a and 3b. During the further cooling to room temperature, OBC1 almost has a spherulite-filled morphology even after annealing at 140 °C for 6 h; on the contrary, OBC4 only formed small, imperfect crystals in the local regions which appear as bright spots in the polarized optical micrographs. To further clarify the morphology of the OBCs in this situation, the samples were further investigated by AFM, as presented in Figure 4. From the AFM images, mesophase separation between hard blocks and soft blocks, as well as the crystalline morphology, can clearly be observed in both OBCs. The structure of OBC4 is dominated by mesophase separation, which appeared as the nearly spherical domains with the diameter of about 100 nm (denoted by the white arrow in Figure 4b), whereas the structure of OBC1 is dominated by lamellae that are degraded in quality by the effect of mesophase separation. These results are consistent with our previous studies.[16]

After blending with iPP, these distinct OBCs caused dramatic difference in crystalline morphology of their blends. When 10 wt %

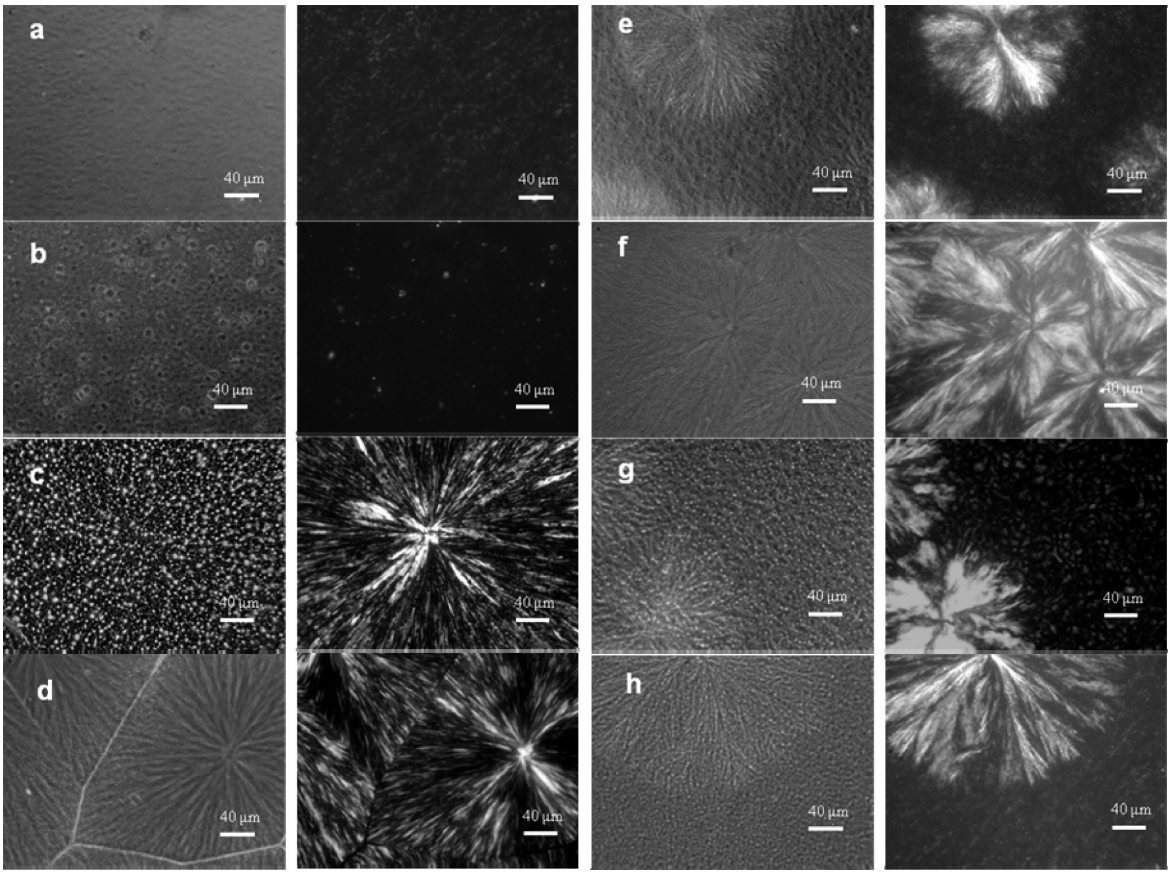

Figure 3. Optical micrographs of samples annealed at 140 °C for 6 h after melting at 200 °C for 5 min: (a) OBC1, (b) OBC4, (c) 1-10, (d) 4-10, (e) 1-90, and (f) 4-90, while (g) and (h) are 1-90 and 4-90 crystallized at 140 °C for 6 h after annealing at 200 °C for 12 h, respectively. All samples were cooled to room temperature at 10 °C/min following the anneal process at 140 °C. The left images are the phase contrast micrographs, and the right ones are the polarized optical micrographs.

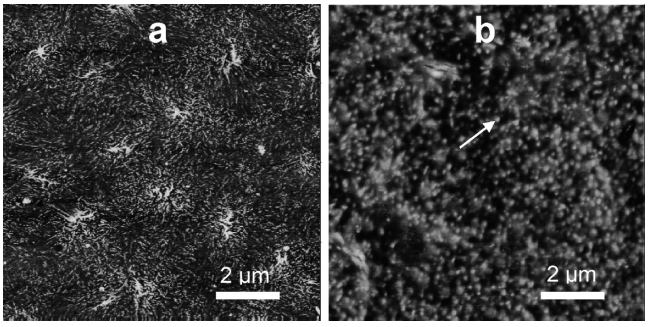

Figure 4. AFM phase images of the OBCs morphology after annealing at 140 °C for 6 h then cooled down to room temperature at 10 °C/min: (a) OBC1; (b) OBC4.

OBC is added to iPP, iPP forms the continuous matrix and OBC forms the dispersed phase. Before crystallization starts, the minor OBC component is already segregated into droplet-like domains in the blend. (The original phase separation morphology at 200 °C of the blends considered obtained by fast quenching will be shown in Figure 5.) During the crystallization process, it appears that the iPP spherulites just grow around the OBC droplets and engulf the latter within the crystals as shown in Figures 3c and 3d. However, it is difficult to distinguish the phase-separated morphology in the phase contrast micrograph for 4-10 in Figure 3d due to the resolution

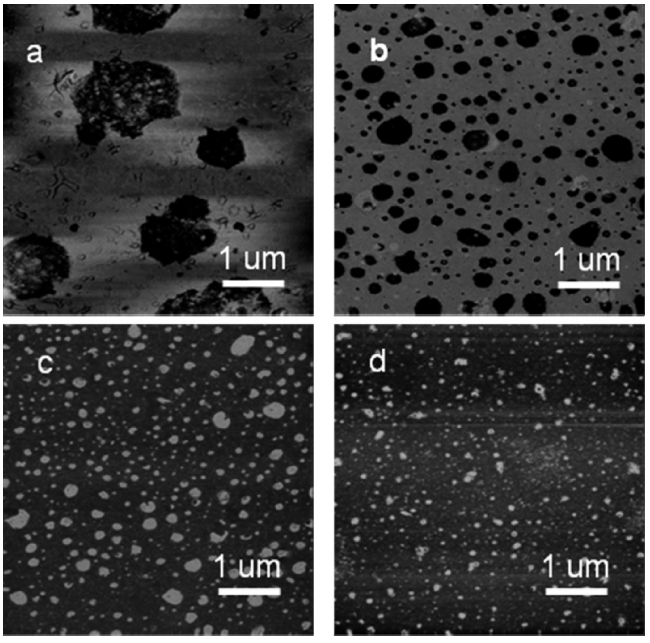

Figure 5. AFM phase images of blends annealing at 200 °C for 5 min followed by rapidly quenching into liquid nitrogen: (a) 1-10, (b) 4-10, (c) 1-90, and (d) 4-90.

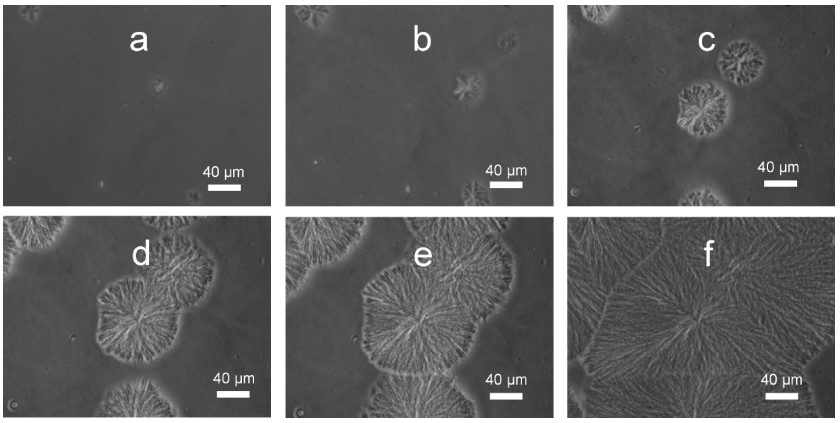

Figure 6. Phase contrast optical micrographs of time-resolved growth process of 4-90 crystallized at 140 °C: (a) 15, (b) 30, (c) 60, (d) 90, (e) 120, and (f) 240 min.

limitations of OM. On the other hand, randomly dispersed OBC-rich droplets that were trapped within the iPP spherulites could be clearly observed for 1-10 in Figure 3c. It should be noted that the OBC domain size in 4-10 is much smaller than 1-10 which indicates the better compatibility between OBC4 and iPP. Reversing the composition of the OBC/iPP blend to 90/10 is likely to invert the phase structure, so that the dispersed domains in 1-90 and 4-90 are the iPP-rich phase and the continuous matrix is the OBC-rich phase, although it is difficult to distinguish the iPP dispersed domains from Figures 3e and 3f. Furthermore, the matrix of OBC should possess a mesophase-separated substructure containing hard block-rich spherical domains dispersed in a soft block-rich matrix. It could be expected that there must be a considerable amount of uncrystallizable impurity held internally within iPP crystals formed at 140 °C, as the matrix phase of OBC was in the molten state in this case. Indeed, the crystalline morphology of iPP in 90/10 OBC/iPP blends displays a dendritic, branchlike texture with an open and irregular profile as shown in Figures 3e and 3f. The structure consists of birefringent (crystalline) arms which are separated by plainly visible interfibrillar layers of OBC phase.

Additionally, by comparing 1-90 and 4-90, the variance between these two blends is obvious. For 1-90, the growth of the dendrite was considerably restrained: after crystallization at 140 °C for 6 h, a significant fraction of the sample volume was still free of iPP crystals. After further cooling to room temperature, OM observations indicated that these noncrystalline regions quickly filled with small crystals (Figure 3e). For 4-90, the dendrites grew much faster and almost completely filled the sample volume under the same condition. Additionally, the iPP was evenly distributed under the micrometer length scale throughout the sample, such that iPP-rich regions were undetectable due to the limit resolution of OM. Moreover, after cooling to room temperature, we expect that any remaining amorphous iPP would crystallize as well as the hard blocks confined within the mesophase-separated domains.

It has been shown that the crystalline morphology of the blends crystallized at 140 °C up to now; however, the original phase structure before crystallization is still unspecified. As quench experiment was an efficient approach to demonstrate the macrophase/microphase separation morphology in the melt, the series of blends for this study were quenched into liquid nitrogen after melting at 200 °C for 5 min, and AFM images were compiled in Figure 5. In 1-10 and 4-10 as shown in Figures 5a and 5b, the dispersed domain is OBC-rich phase. By comparing the dispersed domain size in these two blends after annealing at 200 °C for 5 min, we can conclude that the compatibility of iPP with OBC4 is better than with OBC1. The discrete domains in Figure 5c are more like iPP-rich phase due to the larger dimension; as to Figure 5d, the dispersed phase can either be iPP-rich phase or OBC's mesophase separation domains, which is difficult to distinguish from this AFM image; further evidence for the macrophase separation in 4-90 is shown in Figures 9i and 9j. Still, the better compatibility of iPP with OBC4 is a reasonable explanation for the smaller domain size in Figure 5d than in Figure 5c.

As it is still somewhat surprising that blends containing such a small fraction of iPP could form such dendrite-filled structure, the crystallization process of 4-90 at 140 °C was further investigated with time-resolved OM consequently, as presented in Figure 6. There were obvious crystal nuclei formed even after crystallizing for 15 min, and the micrographs clearly showed the growth of dendrites over time from these nuclei. It is intuitive to detect how the iPP dentrites cover the whole interspace. The fact that 4-90 could crystallize into dendrites filling the entire specimen volume indicates the finer dispersion of iPP chains in the OBC4 matrix.

Moreover, if the iPP dispersed phase grows into a coarser structure prior to crystallization, it can be deduced that the growth of the dendrites will be inhibited due to the decrease of the connectivity among the crystallizable domains. This assumption was confirmed by imposing a phase separation effect before the crystallization process on 1-90 and 4-90. Figures 3g and 3h are the optical micrographs of 1-90 and 4-90 crystallized at 140 °C for 6 h after annealing at 200 °C for 12 h and then cooled down to room temperature, respectively. The iPP macrophase-separated domains as well as the more open and relaxed dendrites structure can be observed from these images, especially for 1-90, where the dispersed iPP-rich macrophase-separated domains after annealing at 200 °C for 12 h were notable from the phase contrast image in Figure 3g. Also, it can be observed that the dendrite crystallized from the much coarser phase separation morphology are more incompact, in this way, the crystalline morphology has been adjusted by tuning annealing conditions. The morphology of 4-90 as shown in Figure 3h is somewhat similar to 1-90 that has been annealed at 200 °C for only 5 min as shown in Figure 3e. Additionally, there was plenty of sample

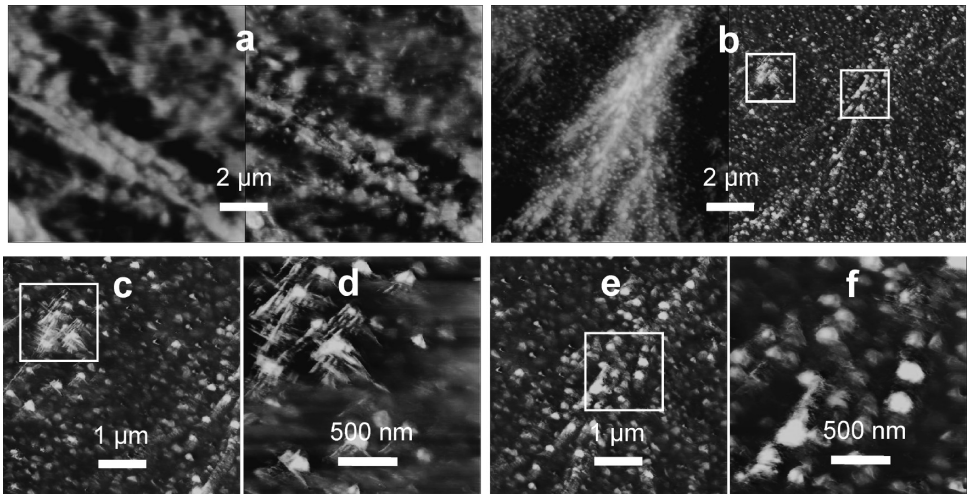

Figure 7. AFM images of 1-90 and 4-90 crystallized at 140 °C for 6 h after annealing at 200 °C for 5 min: (a) height (left) and phase (right) images of 1-90; (b) height (left) and phase (right) images of 4-90, (c) and (e) are the enlarged left and right square parts in (b), respectively; and (d) and (f) are the enlarged square parts of (c) and (e), respectively.

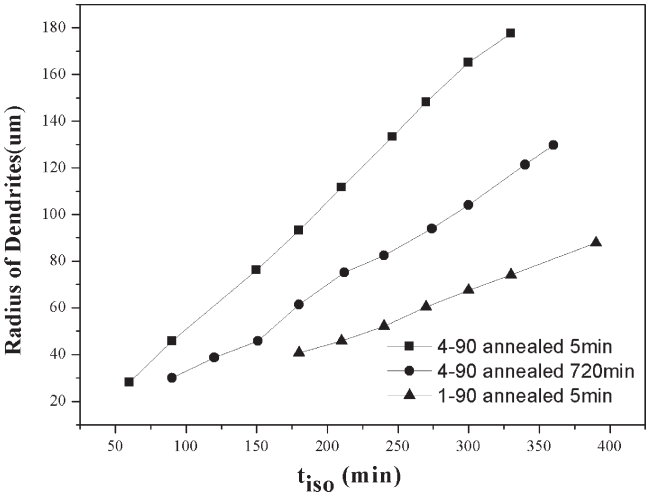

Figure 8. Dendrite growth rate at 140 °C after annealing at 200 °C for 5 min for 1-90 and for 5 and 720 min for 4-90.

volume free of iPP dendrites formed at 140 °C for 6 h, which suggested that the growth rate was decreased greatly compared with the one without long time annealing at 200 °C as shown in Figure 3f. The driving force for macrophase separation between OBC4 and iPP is smaller than that between OBC1 and iPP (as our discussion on χ shown later); therefore, the phase separation rate or the coarsening rate is slower in blend4. It would take longer time for 4-90 to reach to the same sized phase separation morphology as 1-90. However, if we anneal 4-90 for longer time (such as 12 h), it will reach the similar phase-separated domain size and structure compared to 1-90 annealed for only 5 min. Consequently, on the following quenching to 140 °C for isothermal crystallization, the crystallization structure of 4-90 after longer time annealing became similar to that of 1-90 annealing for 5 min.

Evermore, morphology as well as the crystallization kinetics factors was taken into consideration to compare the compatibility in blend1 and blend4: the surface morphology of 1-90 and 4-90 further investigated by AFM is shown in Figure 7, and the growth rate of dendrite is compiled in Figure 8.

The specimens used for AFM were obtained by removing the cover glass of the OM samples in liquid nitrogen. From the height images, the branches of the dendritic crystals are visible, while from the phase images, the simultaneous macrophase separation between iPP and OBC and mesophase separation within the OBC are visible. Figure 7a is the surface morphology of 1-90 showing open-armed iPP dendrites containing loosely packed lamellae, as dictated by the large fraction of noncrystallizable OBC impurity present in the blend. Furthermore, a small population of spherical domains with diameters on the order of several nanometers, corresponding to mesophase separation of the OBC1, is evident in the boundaries between lamellae. However, the mesophase separation of OBC1 appeared in 1-90 was almost negligible when compared to that of OBC4 in 4-90, which is shown in the following.

From both the height and phase images in Figure 7b, a large population of mesophase-separated, spherical domains is apparent in 4-90. These hard block-rich domains of the OBC would be expected to crystallize upon cooling to room temperature after the annealing process. However, we also expect that iPP should macrophase separate into dispersed domains, being the minor component in these blends. There is no doubt that much of the iPP is present in these images as dendritic, albeit highly imperfect crystals; the cross-hatched lamellar structure shown in Figures 7c and 7d is typical of iPP crystallization. Nevertheless, we cannot conclusively rule out the possibility that the small dispersed domains, best depicted in Figures 7e and 7f, consist of some fraction of macrophase-separated iPP. In summary, both these dilute blends formed dendrites with very loose and open armed structure; mesophase separation was more dramatic in 4-90 than 1-90, the larger interspace between lamellar stacks in 1-90 possibly indicating a coarser distribution of iPP-rich, macrophase-separated domains.

To obtain a more quantitative measure about the dendrite growth in these 90/10 OBC/iPP blends, the dendrite growth rate in the 90/10 OBC/iPP blends is presented as a plot of the OM-determined dendrite radius over time in Figure 8. It is clear that the radial growth rate remained almost constant with time in the case of isothermal crystallization at 140 °C. Comparatively, 4-90 has a much faster growth rate than 1-90, which is in good agreement with the

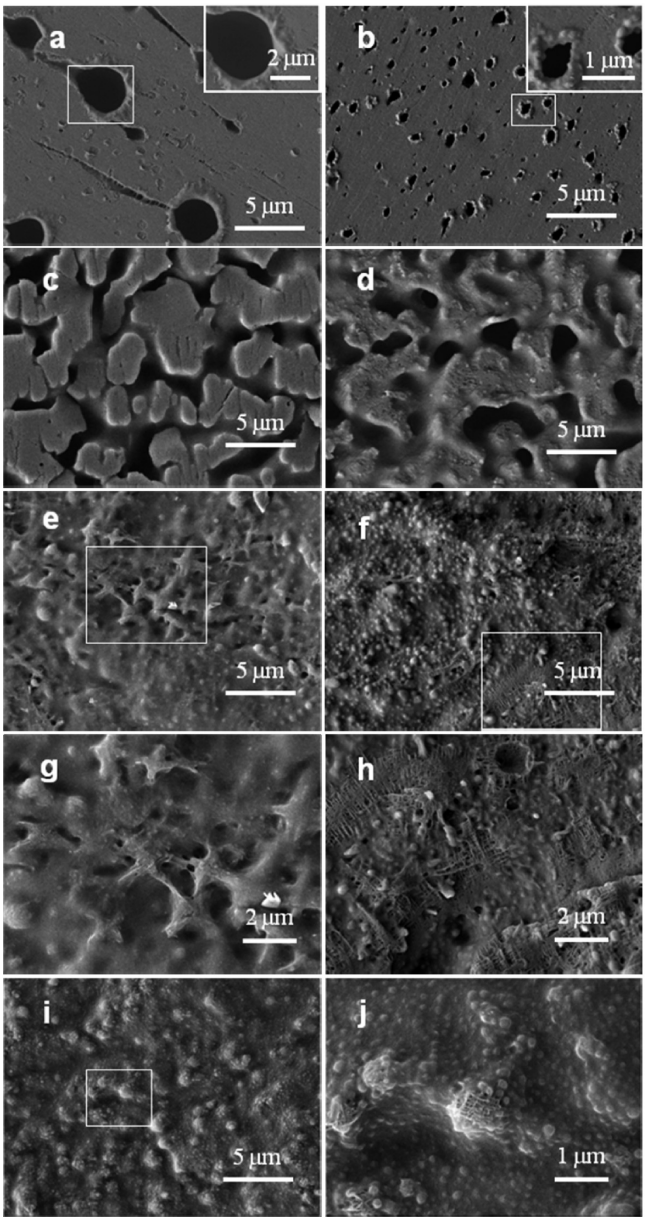

Figure 9. SEM images of blends crystallized at 140 °C for 6 h after annealing at 200 °C for 5 min: (a) 1-10, (b) 4-10, (c) 1-50, (d) 4-50, (e) 1-90, and (f) 4-90; (g) and (h) are magnified images of the solid box in (e) and (f), respectively. These images show the magnified area within an iPP spherulite or dendrite formed at 140 °C. (i) 4-90 crystallized at 140 °C for 6 h after annealing at 200 °C for 12 h. (j) The magnified square part in (i); the area imaged here was selected from the part which was not covered by the iPP dendrite when crystallized at 140 °C for 6 h. All the specimens shown here were cooled down to room temperature following the crystallization at 140 °C.

nonisothermal crystallization behavior mentioned previously further. Moreover, when 4-90 was annealed at 200 °C for 12 h, macrophase separation occurred and the growth rate at 140 °C decreased drastically. The morphology of the dendrite crystallized from the much coarser matrix was once shown in Figure 3h. Combined with the morphology information presented above in Figures 3e, 3f, and 3h, we have further evidence that the growth is retarded with increasing iPP domain size. That 4-90 has a faster growth rate than 1-90 indicates a finer distribution of iPP chains in OBC4 matrix.

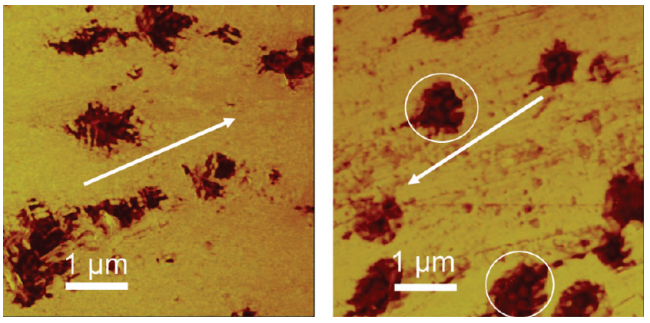

Figure 10. AFM images of unetched samples of 1-10 (left) and 4-10 (right) crystallized at 140 °C for 6 h after annealing at 200 °C for 5 min. The arrow indicates the radial direction of spherulite growth; the white circles on the right highlight the remarkable mesophase separation in OBC4-rich domains.

To further elucidate the morphologies of these blends, all the samples after OM or AFM tests were etched in *n*-heptane for 1 week at room temperature. The SEM images of the etched blends crystallized at 140 °C for 6 h after annealing at 200 °C for 5 min are compiled from Figures 9a to 9h; the left images are for blend1 and the right ones are for blend4. The OBC/iPP blends near phase boundary at 10/90 and 90/10 and with middle at 50/50 components were selected in particular. Since the well-arranged iPP chains are much less soluble in *n*-heptane in this case, the pores in the structure can be attributed to OBC-rich domains. In Figure 9a, the diameters of the pores in 1-10 are more than 3 μm in average. Moreover, these OBC-rich domains were obviously radially deformed as the iPP crystal growth front is prone to reject the rubber phase before engulfing them when crystallizing.[27] From the inset, it can be seen that there is some rubber-like component left at the edge of the pore, which itself is smooth and sharp. In Figure 9b, the pores from 4-10 indicate that the OBC domain size was in the submicrometer range which has been reported as the optimum scale size for mechanical toughing properties. Furthermore, interfacial adhesion was better in this case as the phase boundaries were much rougher in 4-10. Moreover, a small number of egg-shaped objects with 100 nm in diameter can be observed near the edges of the pores, which can be distinguished more clearly in the inset. This structure was confirmed by AFM observation on the same sample without etching, as will be discussed later (Figure 10). Collectively, these results again indicate that OBC4 is more compatible with iPP.

Figures 9c and 9d show a typical spinodal phase separation structure in the iPP spherulite of the OBC/iPP 50:50 blend, and this liquid−liquid phase-separated morphology was almost preserved during the crystallization process. The bicontinuous phase separation structure had already broken into isolated islands in 1-50. In contrast, 4-50 exhibits a well-developed, bicontinuous morphology with highly interconnected iPP and OBC (pore) domains. The distinct morphology in these two blends suggested that 1-50 was in the later phase separation stage than 4-50. Thus, it is supposed that if a macrophase separation process is imposed on 4-50, similar morphology to 1-50 could be achieved. In addition, the interface between the iPP and OBC domains is much rougher in 4-50 than 1-50, as with the 10 wt % OBC blends.

For 1-90, shown in Figures 9e and 9g, it is remarkable that the space within the lamellar stacks is much larger than usual as a great deal of OBC molecules are incorporated into the interlamellar

and/or interfibrillar regions during the crystallization process of iPP, in such a way as to limit its removal during the etching procedure. The relaxed lamellar stacks can be observed clearly, whereas the mesophase-separated domains are not as evident as in 4-90, which is shown in Figures 9f and 9h. For 4-90, there are representative cross hatched lamellar structures. Furthermore, it is obvious to note that the lamellar structure is more compact than in 1-90. Besides the apparent lamellar structure, the remarkable mesophase separation morphology also appears in the matrix of 4-90, which corresponds to the egg-shaped structures with about 100 nm in diameter. The optical micrographs of Figures 3f and 6 have shown that the crystals observed in 4-90 were completely volume-filling even when the iPP content was as low as 10 wt %; in Figures 9f and 9h, the higher resolution SEM images show that the existence of OBC components between the neighbor lamellae spreads the interlamellar distance and leads to a very loose and open armed dendrites structure. The SEM morphology presented here is in reasonable agreement with the AFM results shown in Figure 7. The results further agree in that the macrophase separation of iPP from OBC4 is indiscernible from mesophase separation within OBC4 due to the improved compatibility of iPP and OBC4. It has been shown in Figure 3h that the dendrite was very much restrained when a macrophase separation effect was imposed on 4-90 before crystallization. To further elucidate the macrophase separation morphology in 4-90 annealed at 200 °C, SEM images of this specimen annealed at 200 °C for 12 h were appended in Figures 9i and 9j. The iPP-rich macrophase separation domains can be clearly observed in the images as well as the mesophase separation of the matrix of OBC4, which indicates that 4-90 is a macrophase-separated blend at 200 °C as well.

Returning to Figure 9b, as mentioned, there are many small egg-shaped objects around the boundary of the dispersed phase domains. To exclude the possibility that these structures were faulty images caused by the solvent etching, the sample was investigated by AFM before etching, as shown in Figure 10. It is known that the growth front is prone to reject the rubber phase out of the spherulite during crystallizing.[27] Clearly, the OBC-rich domains were deformed in the radial direction. And this rejection phenomenon is more evident in 1-10 than in 4-10. It is believed that the domain size in 4-10 is much smaller which makes the dispersed OBC-rich domain easier to be engulfed by the iPP crystal growth front without too much deformation. And it is interesting to point out that the smaller egg-shaped objects could be observed clearly within the OBC-rich domains even before etching by solvent, which is much more evident in 4-10 (highlighted in the white circles) than in 1-10. The phenomenon that macro- and mesophase separation both occur in the same system was observed here. We expected that the remarkable mesophase separation in iPP/OBC4 would have some special influence on the iPP/OBC blends.

On the basis of the above results, it could be concluded that the compatibility between iPP and OBC is better in blend4 than in blend1. The improved compatibility must originate from the difference between these two OBCs studied at present.

As the system iPP/OBC considered here is a multiblock copolymer blended with a homopolymer in the absence of a strong reaction (such as ionic and hydrogen bonding effect), the mean-field approximation is applicable here. According to the binary interaction model for a copolymer−homopolymer blend system[28−33]

$$\chi = \chi_{13}\phi_1 + \chi_{23}\phi_2 - \chi_{12}\phi_1\phi_2 \qquad (1)$$

where χ is Flory−Huggins interaction parameter in the blend iPP/OBC system. Here, the subscripts 1, 2, and 3 denote the hard blocks and soft blocks of the OBC and iPP, respectively. ϕ_1 is the volume fraction of hard blocks in OBC, ϕ_2 is the volume fraction of soft blocks in OBC, $\phi_2 = 1 - \phi_1$, and χ_{13} and χ_{23} are the averaged interaction parameters from monomers of hard blocks and soft blocks with those from iPP respectively, and χ_{12} is the interaction parameter between the monomers of the hard blocks and soft blocks "homopolymers".

To reiterate, OBCs differ from anionically polymerized and hydrogenated olefin block copolymers in having a statistical multiblock architecture with a distribution in block lengths and a distribution in the number of blocks per chain.[15] To simplify the problem at present, the hard blocks and soft blocks are represented as equivalent of homopolymers which interact with iPP through a single χ even though both the hard blocks and soft blocks are copolymers.

In addition, we assume that χ_{13} is identical for blends containing OBC1 or OBC4, despite the differing octene content of the hard blocks in those two cases. This is a reasonable assumption because the octene content differs by less than 1 mol % in the hard blocks between OBC1 and OBC4 as well as the hard blocks in both copolymers constitute a small fraction of the total composition seen from the parameters in Table 1. Here, we consider the weight percent is identical to the volume percent. In these two OBCs, the weight percent of hard blocks for both OBCs is similar, so we can neglect the difference in ϕ_1 (or ϕ_2) between blend1 and blend4.

In contrast, there is great distinction between the soft blocks of these two OBCs, as the octene content increased from 23 mol % in OBC1 to 36 mol % in OBC4. Additionally, the weight percent of the soft segments is more than 80%, which would contribute more prominently to the overall χ provided there is significant interaction between the soft blocks and iPP.

There has been considerable effort expended to determine the effect of octene content in ethylene−octene copolymers (EOc) on their compatibility with iPP;[7,11] it was found that the rubber particle size of the blends decreased as the octene content in the EOc was increased, which was a consequence of the reduced interfacial tension between iPP and EOc. Thus, it is reasonable to believe that the soft blocks in OBC4 are more compatible with iPP than in OBC1, which indicates χ_{23} is smaller in blends containing OBC4 than in blends containing OBC1. Additionally, it is known that mesophase separation becomes more dominant as octene content increases in the molecule;[16,34] the more prominent repulsive interaction between the hard and soft blocks in OBC4 suggests a larger χ_{12} compared with OBC1.

In eq 1, when we take into account both the smaller χ_{23} and the larger χ_{12} for blends containing OBC4, while keeping the other numerical value constant, including χ_{13}, ϕ_1, and ϕ_2, we can see easily that the overall χ is smaller, in agreement with our conclusion that there is an enhanced compatibility between iPP and OBC4.

CONCLUSIONS

In this work, the phase behavior of two blends which contain novel OBCs with different octene content in the molecule has been studied in detail. The effect of OBCs' distinct molecular structure on the compatibility of iPP/OBC blends was investigated systematically by comparing the thermal behavior, phase morphology, and kinetics of crystallization.

iPP and OBCs are immiscible in the melt state, and macrophase separation exists in all the components of the iPP/OBC blends. The compatibility between iPP and OBC is dramatically distinct which originates from the difference in octene content of soft blocks in the two OBCs mainly. As the trend of typical mesophase separation effect of these novel OBCs becomes dominant with increasing the octene content, the repulsion effect between the hard blocks and soft blocks enhances mixing between iPP and OBC comparatively. This, coupled with the fact that the majority of soft blocks are more compatible with iPP as octene content increased, leads to better compatibility between iPP and OBC. Consequently, a finer dispersion of iPP-rich (or OBC-rich) domains, improved interfacial adhesion between iPP and OBC domains, and a faster crystal growth rate are obtained in iPP/OBC blends with OBC constituting higher octene content. One the other hand, we found that annealing time plays an important role in controlling the superstructure of the blends. It was shown in our experiments that by imposing a macrophase separation process on blend4, similar morphology and kinetics to blend1 could be obtained as well. Based on our results, a possible scalability of the mesophase separation on the phase behavior of the OBC/iPP blends could be achieved by adjusting the molecular structure of the blocky copolymer and the annealing conditions.

AUTHOR INFORMATION

Corresponding Authors

*E-mail: c.c.han@iccas.ac.cn (C.C.H.); dujiang@iccas.ac.cn (J.D.).

ACKNOWLEDGMENT

This work was supported by National Natural Science Foundation of China (No. 50930003), Young Scientist Fund of NSFC (No. 21004071), and the Ministry of Science and Technology of China special funds for innovative projects in 2009 (2009IM031000). The authors thank The Dow Chemical Company for kindly providing the samples. Jing Jin thanks Brad Jones for kind discussions and revisions.

REFERENCES

(1) Paul, D. R.; Newman, S. *Polymer Blends*; Academic Press: New York, 1978.
(2) Utracki, L. A. *Polymer Alloys and Blends*; Hanser Publishers: New York, 1989.
(3) Vilay, V.; Mariattia, M.; Zulkifli, A.; Pasomsouk, K.; Mitsugu, T. *Mater. Sci. Eng., A* **2010**, *527*, 6930–6937.
(4) Wang, Q.; Wang, X.; Fang, P. F.; Wang, D. H.; Dai, Y. Q.; Wang, S. J.; Liewb, K. M.; Xua, Z. P. *Polym. Int.* **2010**, *59*, 1303–1309.
(5) D'orazio, L.; Mancarella, C.; Martuscelli, E.; Sticotti, G. *J. Mater. Sci.* **1991**, *26*, 4033–4047.
(6) McNally, T.; Mcshane, P.; Nally, G. M.; Murphy, W. R.; Cook, M.; Miller, A. *Polymer* **2002**, *43*, 3785–3793.
(7) Lee, H. Y.; Kim, D. H.; Son, Y. G. *J. Appl. Polym. Sci.* **2007**, *103*, 1133–1139.
(8) Nitta, K.; Kawada, T.; Yamahiro, M.; Mori, H.; Terano, M. *Polymer* **2000**, *41*, 6765–6771.
(9) Lohse, D. J.; Datta, S.; Kresge, E. N. *Macromolecules* **1991**, *24*, 561–566.
(10) Denac, M.; Musil, V.; Šmit, I. *J. Polym. Sci., Part B: Polym. Phys.* **2004**, *42*, 1255–1264.
(11) Liu, G. M.; Zhang, X. Q.; Liu, C. Y.; Chen, H. Y.; Walton, K.; Wang, D. J. *J. Appl. Polym. Sci.* **2011**, *119*, 3591–3597.
(12) Yang, D. C.; Zhang, B. L.; Yang, Y. K.; Fang, Z.; Sun, G. F.; Feng, Z. L. *Polym. Eng. Sci.* **1984**, *24*, 612–617.
(13) Arroyo, M.; Zitzumbo, R.; Avalos, F. *Polymer* **2000**, *41*, 6351–6359.
(14) Arriola, D. J.; Carnahan, E. M.; Hustad, P. D.; Kuhlman, R. L.; Wenzel, T. T. *Science* **2006**, *312*, 714–719.
(15) Shan, C. L. P.; Hazlitt, L. G. *Macromol. Symp.* **2007**, *257*, 80–93.
(16) Jin, J.; Du, J.; Xia, Q. H.; Liang, Y. R.; Han, C. C. *Macromolecules* **2010**, *43*, 10554–10559.
(17) Tucker, P. S.; Barlow, J. W.; Paul, D. R. *Macromolecules* **1988**, *21*, 1678–1685.
(18) Tucker, P. S.; Barlow, J. W.; Paul, D. R. *Macromolecules* **1988**, *21*, 2794–2800.
(19) Matsen, M. W. *Macromolecules* **1995**, *28*, 5765–5773.
(20) Matsen, M. W. *Phys. Rev. Lett.* **1995**, *74*, 4225–4228.
(21) Semenov, A. N. *Macromolecules* **1993**, *26*, 2273–2281.
(22) Bosse, A. W.; Tirumala, V. R.; Lin, E. K. *J. Polym. Sci., Part B: Polym. Phys.* **2009**, *47*, 2083–2090.
(23) Jeong, U.; Ryu, D. Y.; Kho, D. H.; Lee, D. H.; Kim, J. K.; Russell, T. P. *Macromolecules* **2003**, *36*, 3626–3634.
(24) Ruzette, A.-V.; Leibler, L. *Nature Mater.* **2005**, *4*, 19–31.
(25) Zhang, X. H.; Wang, Z. G.; Muthukumar, M.; Han, C. C. *Macromol. Rapid Commun.* **2005**, *26*, 1285–1288.
(26) Zhang, X. H.; Wang, Z. G.; Zhang, R. Y.; Han, C. C. *Macromolecules* **2006**, *39*, 7441–7445.
(27) Keith, H. D.; Padden, F. J. *J. Appl. Polym. Sci.* **1964**, *35*, 1270–1285.
(28) Stockmayer, W. H.; Moore, L. D., Jr.; Fixman, M.; Epstein, B. N. *J. Polym. Sci.* **1955**, *16*, 517–530.
(29) Paul, D. R.; Bucknall, C. B. In *Polymer Blends: Formation and Performance*; Merfeld, G. D., Paul, D. R., Eds.; Academic Press: New York, 1978; Vol. 3.
(30) Kambour, R. P.; Bendler, J. T.; Bopp, R. C. *Macromolecules* **1983**, *16*, 753–757.
(31) Paul, D. R.; Barlow, J. W. *Polymer* **1984**, *25*, 487–494.
(32) Löwenhaupt, B.; Steurer, A.; Hellmann, G. P.; Gallot, Y. *Macromolecules* **1994**, *27*, 908–916.
(33) Zhikuant, C.; Karasz, F. E. *Macromolecules* **1992**, *25*, 4716–4720.
(34) Hustad, P. D.; Marchand, G. R.; Garcia-Meitin, E. I.; Roberts, P. L.; Weinhold, J. D. *Macromolecules* **2009**, *42*, 3788–3794.